Available online at www.sciencedirect.com

SciVerse ScienceDirect

Ceramics International 38 (2012) 1827–1833

CERAMICS INTERNATIONAL

www.elsevier.com/locate/ceramint

# Examining correlations between composition, structure and properties in zircon-containing raw glazes

I. Atkinson [a,b,*], M.E. Smith [b], M. Zaharescu [a]

[a] Institute of Physical Chemistry of the Romanian Academy Bucharest 202 Splaiul Independentei, 060021 Bucharest, Romania
[b] University of Warwick, Department of Physics, Coventry CV4 7AL, UK

Received 6 June 2011; received in revised form 29 September 2011; accepted 3 October 2011
Available online 8 October 2011

**Abstract**

The effects of additions of zircon (5–17 wt%) to conventional single firing ceramic glazes is examined. The structural and morphological characteristics of the glazes were determined by Scanning Electron Microscopy, X-ray diffraction, infra-red spectroscopy, as well as $^{27}$Al and $^{29}$Si magic angle spinning (MAS) NMR. The presence of zircon microcrystals was revealed by X-ray diffraction (XRD) combined with scanning electron microscopy (SEM) and EDAX microanalysis. The chemical durability of the glasses is revealed to be acceptable for certain practical applications. The color characteristics of the glazes obtained were estimated in the HunterLab system ($L^*C^*h^*$, emission spectra). The outcomes of the study established correlations between composition, structure and some of the physical properties.


*Keywords:* C. Chemical properties; D. Traditional ceramics; Glazes; NMR; $ZrSiO_4$

## 1. Introduction

Glazes are commonly applied on surfaces as aqueous suspensions of frits and other additives, also called enamels. Raw glazes are cost-effective alternatives for dense ceramics thermally treated at high top temperatures. Raw glazes are commonly used for sanitary ware and porcelain, and also for frost resistant floor tiles [1,2].

Opaque white glazes are usually obtained in ceramic manufacture from glaze compositions prepared with frits containing $ZrO_2$. In this type of glaze, opacification and whiteness are due to zircon devitrification from the frit during thermal treatment [3,4]. However, the direct incorporation of zircon crystals ($ZrSiO_4$) in the glassy matrix is much more common, due to economic reasons in the case of ceramic products thermally treated at temperatures above 1200 °C. It has a high index of refraction (1.96) and low solubility in glass which makes it a commonly used opacifier for glazes [5,6].

The elimination of the glaze melt fritting process leads to substantial savings in total energy consumption. The phase composition of glazes is usually controlled by the crystallization tendency of the glassy melt during cooling from the firing temperature.

For demanding environments where water impermeability, high mechanical strength, or chemical resistances are required, raw glazes are a competitive alternative to fritted formulations [7]. To interpret their physicochemical properties it is essential to understand the glaze structure which remains a fundamental open question [8]. In the present work the correlation between composition, structure and properties of zircon containing raw glazes is explored.

## 2. Experimental details

### 2.1. Preparation of glazes

Four glazes with 5, 10, 13 and 17% mass fraction of zircon, respectively were studied. The raw materials used for preparation of the glazes were silica, zircon, kaolin, potash feldspar, zinc oxide, wollastonite all of industrial grade. The raw materials in the correct proportions were wet milled up to 0.1% residue using a 63 μm sieve. The material:balls:water

* Corresponding author at: Institute of Physical Chemistry of the Romanian Academy Bucharest, 202 Splaiul Independentei, 060021 Bucharest, Romania. Tel.: +40 21312 11 47; fax: +40 21312 11 47.
*E-mail address:* irinaatkinson@yahoo.com (I. Atkinson).

0272-8842/$36.00 
doi:10.1016/j.ceramint.2011.10.007

Table 1
Oxide compositions of the studied glazes (wt%).

| Sample | $Na_2O$ | $K_2O$ | CaO | ZnO | $Al_2O_3$ | $SiO_2$ | $ZrO_2$ |
|---|---|---|---|---|---|---|---|
| G1 | 1.64 | 3.49 | 10.25 | 1.51 | 11.64 | 68.18 | 3.26 |
| G2 | 1.60 | 3.34 | 9.82 | 1.50 | 11.15 | 66.34 | 6.25 |
| G3 | 1.57 | 3.34 | 9.80 | 1.44 | 10.86 | 63.62 | 9.36 |
| G4 | 1.55 | 3.29 | 9.67 | 1.42 | 10.47 | 61.27 | 12.32 |

ratio was 1:1.5:0.6. The slurry obtained was applied on the green ceramic substrate and thermally treated in an electrical furnace at 1250 °C, with a heating rate of 10 °C/min, where it was held for 1 h and the cooling rate of 5 °C/min. The oxide compositions of the glazes expressed in wt % are presented in Table 1.

### 2.2. Characterization of the glazes

In order to identify the crystalline phases formed during the thermal treatment the glazes were analyzed by X-ray diffraction (XRD). The powdered samples were examined using a Rigaku UltimaIV diffractometer, Cu Kα X-ray radiation, λ = 1.5406 Å, in the 2θ range of 10–80°, step size of 0.02° and scanning speed of 5°/min. The X-ray tube was operated at 40 kV and 30 mA.

The microstructure of the glazes was inspected using a Zeiss SUPRA 55VP Scanning Electron Microscope equipped with energy dispersive X-ray analysis (EDAX) capability.

Infrared transmission spectra were carried out using the same weight of the glaze powder dispersed in KBr pellets. The data were recorded by Nicolet 6700 spectrophotometer in the range 400–1400 $cm^{-1}$.

The $^{29}Si$ magic angle spinning (MAS) NMR spectra were recorded using a Varian InfinityPlus spectrometer with a 7.05 Tesla (T) magnet at a Larmor frequency of 59.6 MHz. The powder samples were packed into 7 mm zirconia rotors and spun at 4 kHz. All the spectra were referenced externally to tetramethylsilane at 0 ppm. The data acquisition conditions were a pulse width of 1.5 μs (corresponding to a tip angle of ∼30°), a pulse delay of 20 s, which produced relaxed spectra for the glassy component, with 800 scans co-added. $^{27}Al$ MAS NMR spectra were recorded using a Bruker Advance $II^+$ spectrometer equipped with a 14.1 T magnet (156.37 MHz for $^{27}Al$). For the experiment the samples were packed into 3.2 mm zirconia rotors and spun at 18 kHz. $Y_3Al_5O_{12}$ (YAG) was used as a reference with the $AlO_6$ resonance set to 0.7 ppm. The data acquisition conditions were a pulse width of 0.7 μs (corresponding to a tip angle of ∼15°), a pulse delay of 1 s with 1800 scans co-added.

The standardized DIN test methods were used to determine the chemical stability of the prepared glazes. The hydrolytic resistance was determined according to DIN ISO 719 (grain-titration method). 2 g of powdered glass with grain size 300–500 μm (ISO) was heated with 50 ml water for one hour in a boiling water bath (98 °C). The extracted alkali is then titrated with hydrochloric acid (HCI) = 0.01 mol/l, using methyl red sodium as the indicator. To determine the acid resistance according to DIN 12116, the glaze surface to be tested is boiled for 6 h in 20% hydrochloric acid [concentration, c (HCI) = 6 mol/l], and the loss in weight is determined in mg/100 $cm^2$. To determine the alkali resistance (DIN ISO 695), glass surfaces are subjected to a 3 h treatment in a boiling aqueous solution consisting of equal volumes of sodium hydroxide, c (NaOH) = 1 mol/l and sodium carbonate, c ($Na_2CO_3$) = 0.5 mol/l.

Color characteristics have been estimated using a MiniScan XE Plus, HunterLab spectrocolorimeter, in 45°/0° optical geometry, with a 4 mm measurement area. *L*a*b** color parameters were measured using a standard lighting C, following the CIE-*L*a*b** colorimetric method recommended by the CIE (Commission Internationale del'Eclairage) [9]. Using this method, *L** is the lightness axis (black (0) white (1 0 0)), *b** is the blue (−) yellow (+) axis, and *a** is the green (−) red (+) axis.

## 3. Results

### 3.1. Structural characterization

#### 3.1.1. X-ray diffraction

Fig. 1 shows the XRD patterns corresponding to the studied glazes. The XRD patterns display the amorphous component with its characteristic hump within the 20–30° 2θ range together with sharp diffraction peaks. The sharp diffraction peaks could be indexed as zircon peaks JCPDS file 01-070-7133 and quartz JCPDS file 00-046-1045.

The crystalline content of the studied glazes was calculated using the XRD deconvolution method. The PeakFit software was used, assuming a Voigt Area G/L function to separate amorphous and crystalline contributions to the diffraction pattern using a curve-fitting process. The crystalline fraction is calculated from the ratio of the area of the crystalline peaks to the total area. A Voigt function is commonly used for deconvolution of such XRD patterns [10]. The results obtained are presented in Table 2.

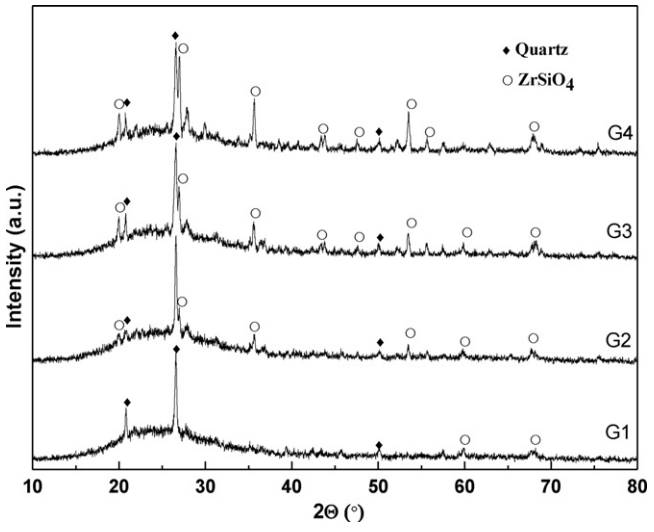


Fig. 1. XRD patterns of the studied glazes.

Table 2
The crystalline fraction of the studied glazes.

| Sample | Crystalline fraction [%] | Amorphous [%] | $r^2$ |
|---|---|---|---|
| G1 | 14 | 86 | 0.960 |
| G2 | 22 | 78 | 0.956 |
| G3 | 31 | 69 | 0.962 |
| G4 | 34 | 66 | 0.984 |

$r^2$ – coefficient of determination ($0 < r^2 < 1$).

### 3.1.2. Scanning electron microscopy

In Figs. 2 and 3(a) the micrographs of glaze–ceramic substrate interfaces for G3 and G4 glazes are presented. SEM investigation of the glaze–ceramic substrate interfaces shows a good adherence of the glaze to the ceramic substrate. Also both un-melted zircon particles as originally added, embedded into the glass matrix, and small acicular crystals that could be assigned to zircon re-crystallized from melt are observed.

In Fig. 3(b) EDAX analysis of the interfacial layer for G4 sample is also presented. The EDAX spectrum of the G4 glaze contains very intense peaks associate to Si, Zr and O indicating the formation of zircon strongly indicating that the opacity of glazes is due to the presence of zircon crystals.

### 3.1.3. Infra-red spectroscopy

Fig. 4 shows the FTIR spectra of the investigated glazes. All obtained spectra show broad bands in the mid-infrared region (1500–400 $cm^{-1}$). The characteristic IR bands of silica are observed in 1038–1062 $cm^{-1}$ range corresponding to the asymmetric vibration of the bridging SiOSi bonds within [$SiO_4$] tetrahedra. Its width is the result of the occurrence in the glass structure of $Q^n$ units, where $Q$ refers to a silica tetrahedron with $n$ bridging oxygens (BO) and $4 - n$ non-bridging oxygens (NBOs) [11]. The band at 784 $cm^{-1}$, is associated with SiO(Si, Al) symmetric stretching vibrations between the tetrahedra. The band at 461 $cm^{-1}$, is due to the bending vibration of SiOSi and SiOAl linkages [12,13]. The band appearing near to 600 $cm^{-1}$ in the case of the G2–G4 samples could be attributed to the Si–O–Zr vibrational modes [14,15]. The asymmetric SiOSi network reported at 1100 $cm^{-1}$ for pure silica shifted to lower frequency suggests that SiOSi is perturbed by the presence of Zr in its environment [16]. All the bands are quite broad and no sharp peaks are observed. This suggests that the glazes studied here exhibit a disordered structure [17].

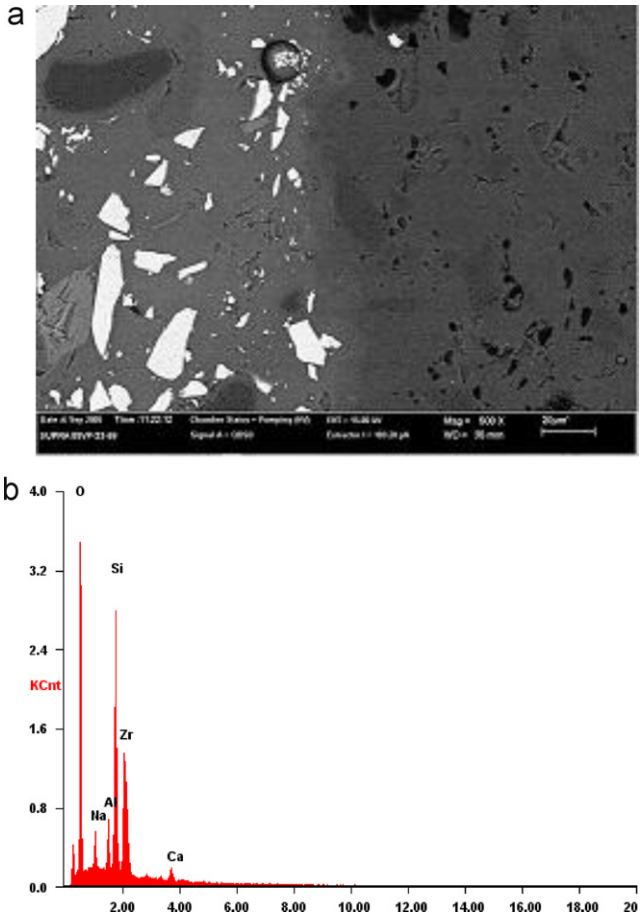


Fig. 3. SEM micrograph (a) of the glaze–ceramic substrate interface for G4 glaze (17 wt% $ZrSiO_4$) and (b) the EDAX result of the interface analysis.

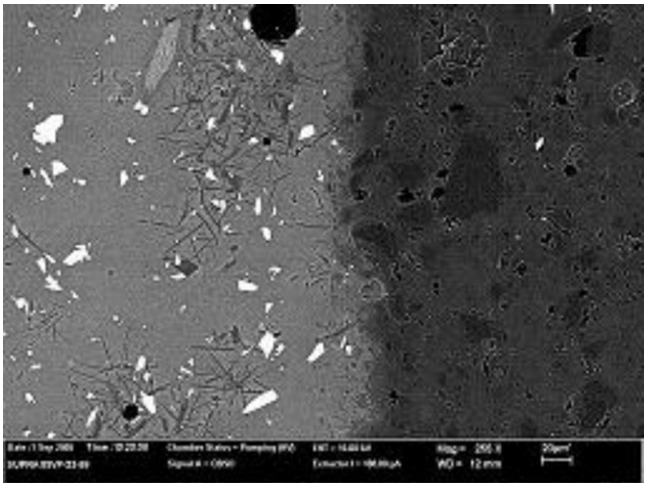

Fig. 2. SEM micrograph of the glaze–ceramic substrate interface for G3 glaze (13 wt% $ZrSiO_4$).

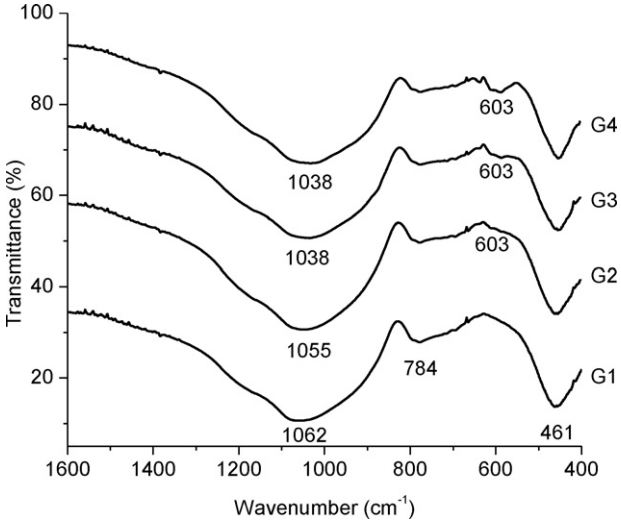


Fig. 4. Infrared spectra of the studied glazes.

Table 3
Solid state $^{29}$Si MAS NMR data.

| Sample | Peak 1 | | | Peak 2 | | | Peak 3 | | |
|---|---|---|---|---|---|---|---|---|---|
| | $\delta \pm 1$ (ppm) | $\Delta \pm 0.5$ kHz | % | $\delta \pm 1$ (ppm) | $\Delta \pm 0.5$ kHz | % | $\delta \pm 1$ (ppm) | $\Delta \pm 0.5$ kHz | % |
| G1 | −100 | 1.19 | 65 | −88 | 1.57 | 35 | – | – | – |
| G2 | −101 | 1.12 | 64 | −88 | 1.17 | 36 | – | – | – |
| G3 | −100 | 1.17 | 70 | −87 | 1.22 | 30 | – | – | – |
| G4 | −100 | 1.13 | 67 | −87 | 0.91 | 26 | −71 | 1.27 | 7 |

$\Delta$ – peak width; $\delta$ – chemical shift.

### 3.1.4. $^{29}$Si MAS NMR

$^{29}$Si MAS NMR spectroscopy provides direct information about the local structure of materials from measurements of the isotropic chemical shift. The chemical shift is influenced by the coordination number of the Si and the number and the type of first cation neighbor. The silicon environment in aluminosilicates can be designated as $Q^n(m\text{Al})$, where $m$ represents the number of attached $AlO_4$ ($m \leq n$) [18]. In aluminosilicate glasses, it is generally concluded that both Si and Al are in tetrahedral coordination to oxygen. These (Si, Al)$O_4$ tetrahedra are corner-sharing through bridging oxygen (BO), forming aluminosilicate frameworks with varying degree of polymerization. The $^{29}$Si MAS NMR spectra for the glazes studied are shown in Fig. 5. The peaks are broad. Very broad lines are observed for highly disordered systems such as amorphous or glassy materials, whereas very much narrower peaks are obtained for perfectly ordered systems [18].

Simulations using two and three Gaussian peaks were performed for the $^{29}$Si NMR spectra using the Dmfit software [19]. The positions, widths and amplitudes of the Gaussians were varied in order to obtain the best fit with the minimum number of peaks. The results are summarized in Table 3. The errors associated with these quantities are determined to be about ±1 ppm for the chemical shift, ±0.5 kHz for the FWHM and ±2% for the intensity. The spectra for G1–G3 glazes have two Gaussian peaks while three Gaussian peaks are necessary to simulate G4 spectra as can be seen in Fig. 6.

The chemical shift of −100 ppm corresponds to $Q^4$(1Al). The peaks at around −88 ppm, could be assigned to $Q^4$(2Al). The peak of −71 ppm could be assigned to $Q^1$. The peaks attributable to the zircon lattice are not observed in the $^{29}$Si NMR spectra for any of the samples (for explanation see Section 4).

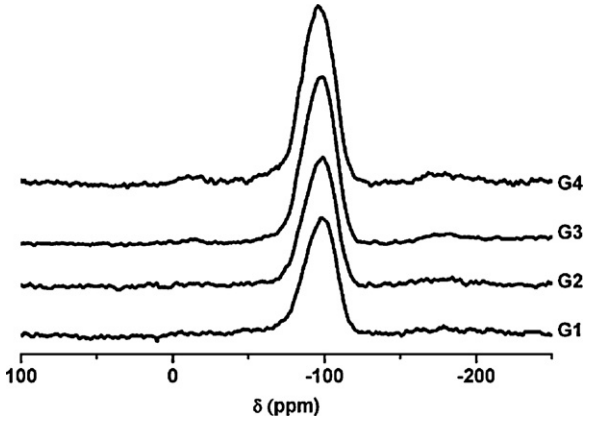


Fig. 5. $^{29}$Si MAS NMR spectra of the studied glazes.

### 3.1.5. $^{27}$Al MAS NMR

The $^{27}$Al NMR spectral data are given in Table 4. The precision and accuracy is about ±1 ppm for the chemical shift and ±2% for the intensity. The FWHM of $^{27}$Al peaks are not reported, because this nucleus experiences second-order quadrupolar peak broadening [20]. The spectra consist of signals from two aluminum environments: that for $AlO_4$ has a maximum at about 53 ppm and that for $AlO_6$ corresponds to 14 ppm. This indicates that the presence of high-coordinated species is likely to be present, in minor amounts, in most aluminosilicate glasses. The same results have been reported for multicomponent oxide systems [21] (Fig. 7).

The structural role of Al is more complex due to the charge balancing requirement of the $AlO_4$ tetrahedra, which is usually achieved by charge compensating alkali or alkaline-earth cations [22]. If such ions are not available for charge compensating the negatively charged $AlO_4$ tetrahedra glass neutrality is then achieved by the Al coordination change to a higher number that assumes a positive charge. Non-framework cations such as Ca and Na can act as either charge-balancing or network modifying cations, depending on the overall composition. The network modifying cations lead to the formation of non-bridging oxygen (NBO) thereby decreases the extent of polymerization.

## 3.2. Properties of glazes

### 3.2.1. Chemical stability

The chemical durability of glazes studied in hydrolytic, acidic and alkali solutions is given in Table 5.

The results obtained from chemical stability study of the glazes show that the investigated glazes have good hydrolytic

Table 4
Solid state $^{27}$Al MAS NMR data.

| Sample | Peak 1 | | Peak 2 | |
|---|---|---|---|---|
| | $\delta \pm 1$ (ppm) | % ±2 | $\delta \pm 1$ (ppm) | % ±2 |
| G1 | 53 | 86 | 14 | 14 |
| G2 | 54 | 87 | 15 | 13 |
| G3 | 53 | 82 | 14 | 18 |
| G4 | 53 | 74 | 14 | 26 |

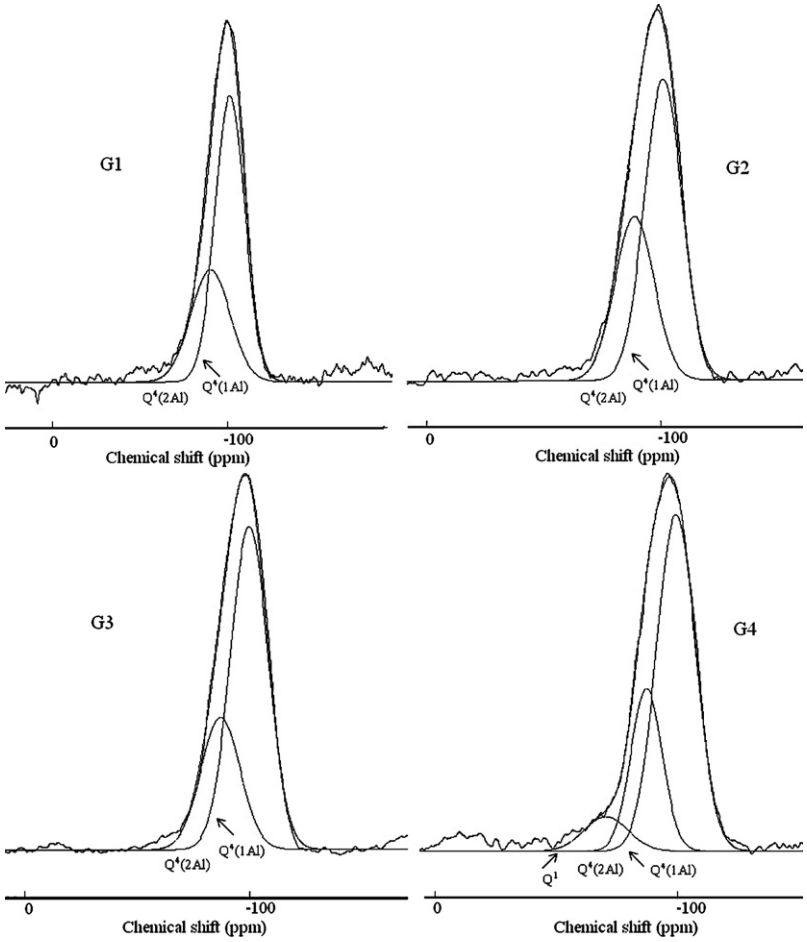


Fig. 6. Deconvoluted $^{29}$Si MAS NMR spectra of the glazes showing the Gaussians fitted to the different $Q$ species present.

and alkali resistance (class 1). According to the acid resistance test the glazes are classified as follows: G1 and G2 glazes are slightly attacked by acid while glazes G3 and G4 are acid resistant.

### 3.2.2. Optical properties

The CIELab parameters of the samples are given in Table 6.

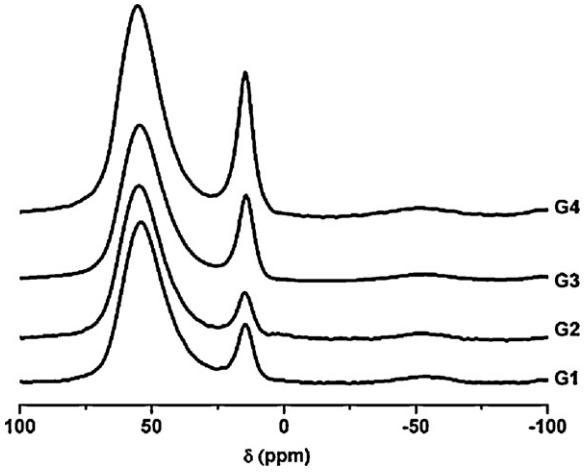


Fig. 7. $^{27}$Al MAS NMR spectra of the studied glazes.

As can be seen, the glazes present high lightness value ($L^*$) typical of opaque glazes. The lightness value, which is a measure of reflectivity, close to 100 shows a good reflecting surface. The best quality glazes are obtained when the color of the ceramic substrate cannot be seen through the glaze and the appearance of the piece is white. The samples are also characterized by lower values of $a^*$ and $b^*$, indicating a tendency to achromatism.

The total reflectance depends on the glaze thickness, the presence of crystalline phases in the glaze and the body color. No significant differences were observed in the reflectance curves of the G1, G2 and G4 samples (Fig. 8). The reflectance of the G3 (13 wt% $ZrSiO_4$) glaze is higher than the others indicating a better light diffusion due to the smaller particles size of zircon in glaze.

## 4. Discussion

X-ray diffraction shows the preponderantly amorphous character of the studied glazes. The SEM-EDAX analysis and XRD patterns confirm that in the prepared glazes in this study un-melted and devitrified zircon crystals responsible of the opaque proprieties of the obtained glazes exist.

The following possibilities exist when zircon is used in a glaze: the zircon crystals can be stable and be unaffected by the glaze during firing, the zircon particles can partially or totally

Table 5
Chemical stability of the glazes.

| Sample | Hydrolytic resistance | | Acid resistance | | Alkali resistance | |
|---|---|---|---|---|---|---|
| | $Na_2O$ released/g glass grain (mg × $10^{-2}$) | Hydrolytic class | Half loss in weight after 6 h mg/cm$^2$ | Acid class | Loss in weight after 3 h mg/cm$^2$ | Alkali class |
| G1 | 2 | 1 | 2.8 | 3 | 54.4 | 1 |
| G2 | 1.8 | 1 | 2.7 | 3 | 41.4 | 1 |
| G3 | 1.6 | 1 | 1.5 | 2 | 34.3 | 1 |
| G4 | 1.4 | 1 | 1.1 | 2 | 14.8 | 1 |

dissolve in the glaze during firing with the dissolved portion either remaining or re-crystallizing from the melt.

FT-IR spectra confirm the results obtained by XRD and SEM, and show that G2–G4 glazes have supplementary vibration bands characteristic of SiOZr vibrational modes. The shift of the main band maximum from 1100 cm$^{-1}$ to lower frequencies suggests that SiOSi is perturbed by the presence of Zr in its environment. In the FT-IR spectra the crystalline phases identified by XRD and SEM are overlapped by the broad band of the vitreous component. The IR band of Si–O–Zr is identified at 603 cm$^{-1}$ and the intensity of the band increases with the amount of $ZrSiO_4$ introduced.

$^{29}$Si MAS NMR data show that the glazes are highly disordered and the silicon is contained within the glassy phase. The small amount of crystallized quartz observed by XRD could not be identified by NMR due to the overlapping of its chemical shift with that of the $^{29}$Si from the vitreous matrix, but more importantly probably due to the much longer $T_1$ relaxation time observed in some crystalline systems especially for spin-1/2 nuclei such as $^{29}$Si[18]. Although XRD and SEM show the presence of zircon there are no peaks caused by Zr–O–Si bonds present in the corresponding $^{29}$Si MAS NMR spectra, again almost certainly due to the very long relaxation time of this crystalline component causing very strong saturation of this signal under the conditions used [23,24].

Aluminum largely acts as a network former in these glazes, with the majority of the aluminum present as $AlO_4$, but also to some extent as a network modifier ($AlO_6$ form). This observation is very much in keeping with its intermediate behavior. It is interesting to note what the effect of the changing composition is in terms of the structure of the amorphous matrix component. The metal content (other than the zirconium) remains approximately constant. Some of the silicon will be required to form the zircon, which leaves less to form the amorphous network. Hence there is a higher aluminum content left as part of the network and in G4 there is some lower n $Q^n$-species observed (probably $Q^1$). This then means the network carries more negative charge which sees more aluminum occupying octahedral coordination (hence contributing positive charge).

The influence of the composition and structure of the glazes obtained on their properties were evaluated by chemical stability tests and color measurements.

Chemical durability of glazes is often discussed in terms of the durability of the glassy phase. The early stages of glaze leaching, called ''inter diffusion'', correspond to a fast ion exchange involving mobile glaze components ($Na^+$) and protons from the solution. At the same time, the hydrolysis of the glassy network begins at a lower rate, modifying the Si–O–(Si, Al) bonds. The difference between the kinetics of these two simultaneous processes leads to the formation of a porous and hydrated layer at the glaze/water interface [25–27].

In acidic solutions hydrogen ions are assumed to replace the modifier ions in the glass network while in alkaline solutions the silica network is attacked. The glassy phase is assumed to react similarly to conventional glasses, i.e. with ion-exchange of alkali ions in acidic environments [28]. $Al_2O_3$, MgO and $ZrO_2$ are known to form structural building groups in the glaze which improve the chemical durability. The alkali ions compensate for the negative charge associated with parts of the network such as $AlO_4^-$ and in such a role these alkali ions are tightly bound and cannot be readily detached during the corrosion process. Chemical stability results show that all the glazes have good hydrolytic and alkali resistance (class 1). The glazes with higher content of $ZrSiO_4$ (G3 and G4) are acid resistant. Zircon is widely known to improve the durability of

Table 6
$L^*$, $a^*$, $b^*$ parameters of the studied glazes.

| Sample | $L^*$ | $a^*$ | $b^*$ |
|---|---|---|---|
| G1 | 89.00 | −0.87 | 4.19 |
| G2 | 89.00 | −0.86 | 3.92 |
| G3 | 91.00 | −0.77 | 3.80 |
| G4 | 90.00 | −0.32 | 3.50 |

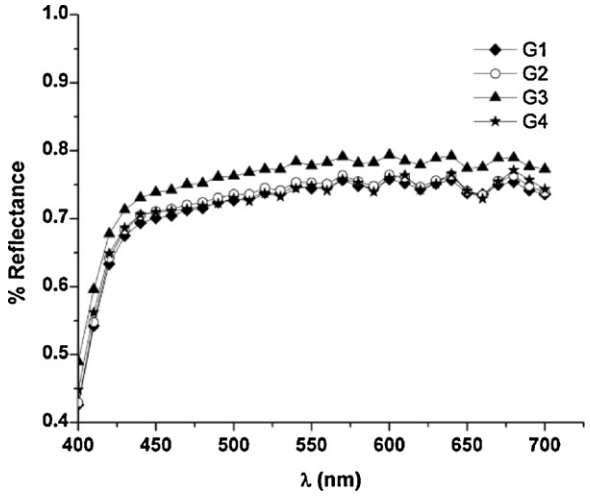


Fig. 8. Reflectance curves of the glazes.

glazes more than any other element. Even small concentration of zircon (2%) yield significant improvements in both acid and alkaline durability. Although the hydration of $ZrO_2$ is energetically favorable soluble ionic species like $ZrO^{2+}$, $Zr^{4+}$ and $HZrOO_3^-$ occur only below pH 2 and above pH 17 [29].

The optical properties of an object depend on the interaction of the radiation at every wavelength (reflectance) that is a function of the absorbed and scattered light. This means that for each frequency in the visible all the components of the glaze (pigments, opacifiers and crystals formed from frit) have both absorption and scattering coefficients, each one contributing to the optical properties of the glaze. However all glazes showed a good reflecting surface.

## 5. Conclusions

In this paper the influence of the composition on the structure and properties of zirconium-containing glazes was investigated. SEM-EDAX analysis and XRD revealed the presence of $ZrSiO_4$ crystals which contribute to the opacity and enhance some properties of the final glazes. $^{29}$Si MAS NMR data show that the bulk of the silicon in the glazes is highly disordered; hence the silicon is contained mainly within the glassy phase. $^{27}$Al MAS NMR data shows that aluminum acts both as a network former as well as a network modifier in these glazes. The presence of $ZrSiO_4$ improved the chemical stability of the studied glazes. The color measurements of the glazes showed the all glazes present high lightness value ($L^*$), typical of opaque glazes which suggests a good reflecting surface.

## Acknowledgements

I. (Gresoiu) Atkinson gratefully acknowledges the financial support from the European Commission for a Marie Curie scholarship "Solid State NMR of Inorganic Materials" to the University of Warwick, UK as part of an Early Career Training Site. Warwick's NMR facility is partially supported by the University of Warwick and EPSRC whose contributions are gratefully acknowledged.

## References

[1] M.G. Rasteiro, T. Gassman, R. Santos, E. Antunes, Crystalline phase characterization of glass–ceramic glazes, Ceram. Int. 33 (2007) 345–354.
[2] L. Froberg, T. Kronberg, L. Hupa, M. Hupa, Influence of firing parameters on phase composition of raw glazes, J. Eur. Ceram. Soc. 27 (2007) 1671–1675.
[3] E. Bou, A. Moreno, A. Escardino, A. Gozalbo, Microstructural study of opaque glazes obtained from frits of the system: $SiO_2$–$Al_2O_3$–$B_2O_3$–($P_2O_5$)–CaO–$K_2O$–$TiO_2$, J. Eur. Ceram. Soc. 27 (2007) 1791–1796.
[4] L.M. Schabbach, F. Bondioli, A.M. Ferrari, T. Manfredini, C.O. Petter, M.C. Fredel, Influence of firing temperature on the color developed by a (Zr V)$SiO_4$ pigmented opaque ceramic glaze, J. Eur. Ceram. Soc. 27 (2007) 179–184.
[5] M. Lusar, G. Monros, C.M. Rodrigues, J.A. Labrincha, Study of zircon or zirconia crystals addition in ceramic glazes by impedance spectroscopy, Ceram. Int. 31 (2005) 181–188.
[6] L.M. Schabbach, F. Bondioli, A.M. Ferrari, C.O. Petter, M.C. Fredel, Colour in ceramic glazes: efficiency of the Kubelka–Munk model in glazes with a black pigment and opacifier, J. Eur. Ceram. Soc. 29 (2009) 2685–2690.
[7] L. Fröberg, T. Kronberg, L. Hupa, Effect of soaking time on phase composition and topography and surface microstructure in vitrocrystalline whiteware glazes, J. Eur. Ceram. Soc. 29 (2009) 2153–2161.
[8] G. Calas, L. Cormier, L. Galoisy, P. Jollivet, Structure–property relationships in multicomponent oxide glasses, C. R. Chim. 5 (2002) 831–843.
[9] CIE, Recommendations on uniform colour spaces, colour difference equations, psychometrics colour terms, in: Suplement n 2 of CIE Publ. N 15 (E1-1. 31) 1971, Bureau Central de la CIE, Paris, 1978.
[10] S. Park, J. O' Baker, M.E. Himmel, P.A. Parilla, D.K. Johnson, Cellulose crystallinity index: measurement techniques and their impact on interpreting cellulase performance, Biotechnol. Biofuels 3 (2010) 1–10.
[11] M. Sroda, Cz. Paluszkiewicz, The structural role of alkaline earth ions in oxyfluoride aluminosilicate glasses—infrared spectroscopy study, Vib. Spectrosc. 48 (2008) 246–250.
[12] F.H. ElBatal, M.A. Azooz, Y.M. Hamdy, Preparation and characterization of some multicomponent silicate glasses and their glass–ceramics derivatives for dental applications, Ceram. Int. 35 (2009) 1211–1218.
[13] C.I. Merzbacher, K.J. McGrath, P.L. Higby, $^{29}$Si NMR and infrared reflectance spectroscopy of low-silica calcium aluminosilicate glasses, J. Non-Cryst. Solids 136 (1991) 249–259.
[14] M. Popa, J.M. Calderón-Moreno, L. Popescu, M. Kakihana, R. Torecillas, Crystallization of gel-derived and quenched glasses in the ternary oxide $Al_2O_3$–$ZrO_2$–$SiO_2$ system, J. Non-Cryst. Solids 297 (2002) 290–300.
[15] M. Popa, M. Kakihana, M. Yoshimura, J.M. Calderon-Moreno, Zircon formation from amorphous powder and melt in the silica-rich region of the alumina–silica–zirconia system, J. Non-Cryst. Solids 352 (2006) 5663–5669.
[16] J. Chandradass, K.S. Han, D.S. Bae, Synthesis and characterization of zirconia and silica-doped zirconia nanopowders by oxalate processing, J. Mater. Process. Technol. 206 (2008) 315–321.
[17] B.N. Roy, Infrared spectroscopy of lead and alkaline-earth aluminosilicate glasses, J. Am. Ceram. Soc. 73 (1990) 846–855.
[18] K.J.D. MacKenzie, M.E. Smith, Multinuclear Solid State NMR of Inorganic Materials, Pergamon Press, Oxford, 2002.
[19] D. Massiot, F. Fayon, M. Capron, I. King, S.L. Calvé, B. Alonso, J.O. Durand, B. Bujoli, Z. Gan, G. Hoatson, Modelling one and two-dimensional solid state NMR spectra, Magn. Reson. Chem. 40 (2002) 70–76.
[20] M.E. Smith, E.R.H. Van Eck, Recent advances in experimental solid state NMR methodology for half-integer spin quadrupolar nuclei, Prog. Nucl. Magn. Reson. Spectrosc. 34 (1999) 159–201.
[21] I. Atkinson, I. Teoreanu, O.C. Mocioiu, M.E. Smith, M. Zaharescu, Structure–property relations in multicomponent oxide systems with additions of $TiO_2$ and $ZrO_2$ for glaze applications, J. Non-Cryst. Solids 356 (2010) 2437–2443.
[22] D.R. Neuville, L. Cormier, V. Montouillout, D. Massiot, Local Al site distribution in aluminosilicate glasses by $^{27}$Al MQMAS NMR, J. Non-Cryst. Solids 353 (2007) 180–184.
[23] I. Farnan, E.K.H. Salje, The degree and nature of radiation damage in zircon observed by Si-29 nuclear magnetic resonance, J. Appl. Phys. 89 (2001) 2084–2090.
[24] N. Dajda, J.M. Dixon, M.E. Smith, N. Carthey, P.T. Bishop, Atomic site preferences and structural evolution on vanadium-doped $ZrSiO_4$ from multinuclear solid state NMR, Phys. Rev. B 67 (2003) 024201.
[25] B. Bergeron, L. Galoisy, P. Jollivet, F. Angeli, T. Charpentier, G. Calas, S. Gin, First investigations of the influence of IVB elements (Ti, Zr and Hf) on the chemical durability of soda-lime borosilicate glasses, J. Non-Cryst. Solids 356 (2010) 2315–2322.
[26] L. Sicard, O. Spalla, O. Né, F. Taché, P. Barboux P, Dissolution of oxide glasses: a process driven by surface generation, J. Phys. Chem. C 112 (2008) 1594–1603.
[27] G. Geneste G., F. Bouyer, S. Gin, Hydrogen–sodium interdiffusion in borosilicate glasses investigated from first principles, J. Non-Cryst. Solids 352 (2006) 3147–3152.
[28] L. Froberg, T. Kronberg, S. Tornblom, L. Hupa, Chemical durability of glazed surfaces, J. Eur. Ceram. Soc. 27 (2007) 1811–1816.
[29] R.A. Eppler, D.A. Eppler, Glazes and Glass Coatings, The American Ceramic Society Westerville, Ohio, 2000.